PMD Measurement Techniques – Avoiding Measurement Pitfalls

P.A. Williams
National Institute of Standards and Technology,
325 Broadway, Boulder, CO 80305,
paul.williams@nist.gov

I. Introduction

Measuring polarization-mode dispersion (PMD) can be confusing. Many different techniques for PMD measurement are available, and often many user-selectable parameters are associated with the measurement. This presentation will describe the various measurement methods and discuss the "best practices" for measurements with each method.

II. What Does it Take to Describe PMD?

The PMD of a device is completely described when the Differential Group Delay (DGD) and the Principal States of Polarization (PSP) are characterized as functions of wavelength. Often, the terms PMD and DGD are used interchangeably, but here we will use the term PMD to describe the phenomenon and DGD to describe its magnitude. Both the DGD and the PSP are contained in the 3-dimensional polarization dispersion vector $\Omega(\lambda)$. The DGD is given by the magnitude $\Delta\tau = |\Omega|$, and the PSP are given by the direction of Ω. For many applications, only $\Delta\tau(\lambda)$ is needed, and often even the wavelength dependence is not measured, in which case PMD is reported as the wavelength-averaged DGD $\langle\Delta\tau\rangle_\lambda$ or the root-mean-square (RMS) value $\langle\Delta\tau^2\rangle_\lambda^{1/2}$.

In order to describe the various measurement techniques, we will discuss the two general cases of PMD–devices with and without polarization-mode coupling. A "non-mode-coupled" device is a simple birefringent element such as a single birefringent crystal. In this case, the polarization eigenaxes of the device coincide with the PSP and are independent of wavelength, and $\Delta\tau$ is only weakly dependent on wavelength. For example, in quartz, $\Delta\tau$ changes by less than 3 % over the 1300-1800 nm wavelength range (Figure 1) [1]. In "mode-coupled" devices, the eigenaxes do not necessarily coincide with the PSPs. The PSPs are independent of wavelength only to first order, and $\Delta\tau$ can be strongly dependent on wavelength (Figure 2).
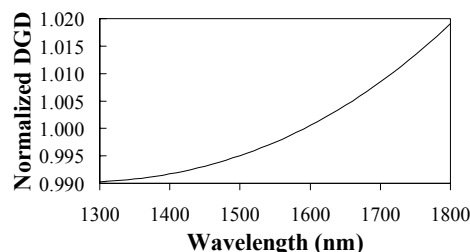

Figure 1. Normalized DGD spectrum for quartz.

Exactly what must be measured in order to characterize the PMD of a device depends on the degree of mode coupling of the device and on what the measurement will be used for. Often, for non-mode-coupled devices, the mean DGD is well-approximated by the DGD at a particular wavelength $\langle\Delta\tau\rangle \approx \Delta\tau(\lambda)$, and so the DGD needn't be resolved as a function of wavelength. On the other hand, for mode-coupled devices, such as long lengths of fiber, $\langle\Delta\tau\rangle$ and $\Delta\tau(\lambda)$ can be very different. However, if only the average behavior of the device is of concern, then the mean (or RMS) DGD may suffice.
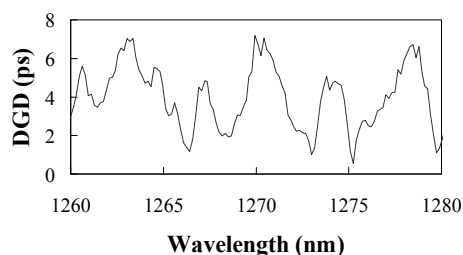

Figure 2. Sample DGD spectrum of a mode-coupled device.

In highly mode-coupled fibers, $\Delta\tau$ exhibits a large variance as the wavelength, temperature, stress, fiber position, or other environmental parameters change. So, in order to accurately report the mean DGD of a mode-coupled device, it is necessary to also report the uncertainty due to this variance of $\Delta\tau$. Gisin et al. have demonstrated that four major PMD measurement techniques are subject to the same level of uncertainty

due to this statistical variation of the DGD in mode-coupled devices [2]. And, it is usually assumed that the variance applies to all techniques. If a fiber of mean DGD $\langle\Delta\tau\rangle$ is measured over a bandwidth of $\Delta\omega_{span}$, then the standard deviation σ, normalized to $\langle\Delta\tau\rangle$, is given by [2]

$$\frac{\sigma}{\langle\Delta\tau\rangle} \approx \frac{1}{\sqrt{\langle\Delta\tau\rangle\Delta\omega_{span}}}. \qquad (1)$$

For highly mode-coupled devices, $\sigma/\langle\Delta\tau\rangle$ decreases when larger values of DGD are measured or the average is made over a wider spectral bandwidth (or equivalently over more statistically independent samples).

The various measurement techniques can be classified as either time-domain or frequency-domain techniques. The clearest separation between the two is seen in the relationship between the coherence time T_c of the measurement light and $\Delta\tau$ (the DGD being measured). A technique is considered to be in the time domain if $T_c < \Delta\tau$, and in the frequency domain if $T_c > \Delta\tau$. The descriptions of the different techniques will, of course, be abbreviated, but helpful details can be found in Reference [3].
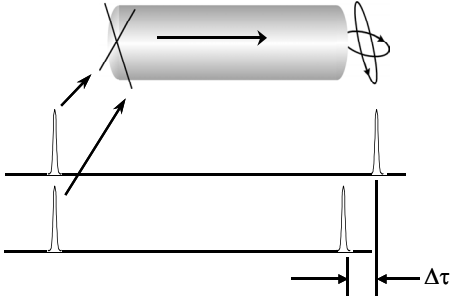

Figure 3. Diagram of input pulses launched simultaneously down the fast and slow PSP of a device. Output pulses emerge at different times corresponding to the difference in group delay.

III. Time-Domain Measurements

Time of flight: The time-of-flight measurement is the most intuitive, so we will consider it first. Figure 3 illustrates a narrow pulses of light transmitted through a non-mode-coupled device of DGD $\Delta\tau = \tau_f - \tau_s$. The propagation delay through the device will be either be τ_f (if the input pulse is po-larized along the fast PSP), τ_s (if it is polarized along the slow PSP), or if the polarization state of the pulse is between the fast and slow PSP, the pulse will be broken into two pulses with delays τ_f and τ_s, with relative intensities weighted according to the orientation of the input polarization state with respect to the fast and slow PSP. So, in this intuitive measurement technique, short optical pulses are launched into a test device and detected at the output. A fast oscilloscope plots the arrival time of the pulses as the input polarization state is changed. For launch polarizations between the two PSP, two received pulses are seen separated in time by the mean DGD (averaged over the spectral bandwidth of the pulses). This technique is well known [4-6], but is often impractical since the pulse width limits the temporal resolution (requiring narrow pulse widths on the order of the desired DGD resolution).
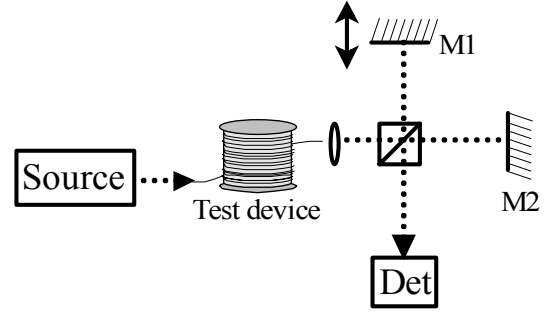

Figure 4. Schematic diagram of low-coherence interferometer: M1 is the movable mirror.

Low-Coherence Interferometry: A closely related but more practical approach to time-domain measurement is through low-coherence interferometry (Figure 4). A spectrally broad (low-coherence) source sends light through the test device and into an interferometer. As the moveable arm of the interferometer is translated, interference fringes are seen at the detector only if the time-delay difference between the two arms matches a delay generated in the test device to within the coherence time of the source. Ignoring possible coherence effects, this condition can be written simplistically as

$$\left|(\tau_{arm,1} - \tau_{arm,2}) - (\tau_i - \tau_j)\right| < T_C, \quad (2)$$

where $\tau_{arm,1}$ and $\tau_{arm,2}$ are the time delays associated with propagation along each arm

of the interferometer, τ_i and τ_j are two possible propagation times experienced by light traveling along the ith and j^{th} polarization paths through the device. T_c is the coherence time of the source (e.g. for a Gaussian source of spectral width $\Delta\lambda$ and center wavelength λ, $T_C = 0.664 \cdot \lambda^2 / c\Delta\lambda$, c is the speed of light) [7]. Equation (2) gives an intuitive picture of the interferogram shape. For the non-mode-coupled case, there are only two nondegenerate paths through the device–light traveling along the fast axis or along the slow axis. So, the only possible values of the difference $\tau_i - \tau_j$ are 0 or $\pm\langle\Delta\tau\rangle_\lambda$, where $\langle\Delta\tau\rangle_\lambda$ is the result of an average of the DGD over the spectrum of the source, weighted by the intensity of the source at each wavelength.
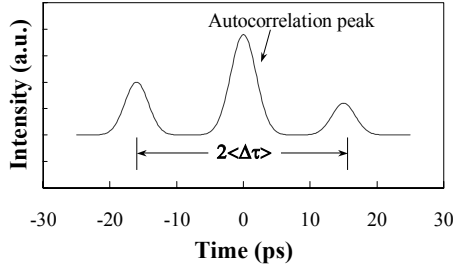

Figure 5. Sample interferogram envelope for a non-mode coupled device.

Plotting the envelope of interference fringes as the moveable arm of the interferometer is scanned gives a delay histogram similar to Figure 5 for a non-mode-coupled device. The central peak of the delay histogram is the autocorrelation of the source, which does not give any information about the strength of the PMD ($\tau_i - \tau_j = 0$). The two side lobes are separated from the autocorrelation peak by an amount $\langle\Delta\tau\rangle_\lambda$. So, for non-mode-coupled devices, measuring the separation of the side lobes gives $2\langle\Delta\tau\rangle_\lambda$.

The width of the peak at 0 is equal to the coherence time of the source and provides the temporal resolution limit. In other words, if the PMD is too low, the side-lobe separation will be less than the coherence time of the source, causing the side lobes to add coherently with the central peak, making it impossible to identify their position. This illustrates the tradeoff between bandwidth and DGD resolution; a broader

source gives a better DGD resolution, but at the expense of the spectral resolution of the DGD.

The finite width of the peaks at $\pm\langle\Delta\tau\rangle_\lambda$ comes from two separate causes. First, the coherence time of the source broadens the peak. Second, the value of $\Delta\tau$ is not constant over the source spectrum, so there is some broadening of the peak due to variation of DGD with wavelength.
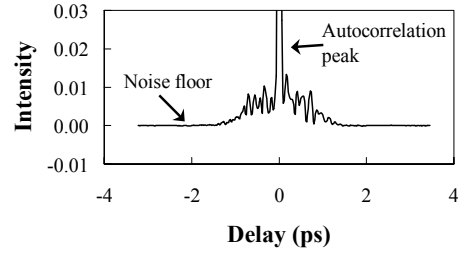

Figure 6. Sample interferogram envelope for a mode-coupled device.

Low-coherence interferometry can be used to measure mode-coupled devices as well. In this case, τ_i and τ_j can take on 2^{N+1} different values (where N is the number of mode-coupling sites in the artifact). This yields a delay histogram with $2^{N+2}-1$ peaks. However, the separation of adjacent peaks can easily be less than the coherence time of the source and so the peaks are not necessarily distinguishable. The resulting interferogram envelope comes from the coherent addition of the various delays. Figure 6 gives an example delay histogram for a highly mode-coupled device. In highly mode-coupled devices, it is customary to characterize the root-mean-square (RMS) value of the DGD over the wavelength range of the measurement. The "second moment"

$$ \sigma_M = \sqrt{\frac{\int I(t)t^2 dt}{\int I(t)dt}} \qquad (3) $$

of this Gaussian-shaped delay histogram will generally[†] yield the RMS DGD value

---

[†] Equation (4) assumes a large DGD-source-bandwidth product. When the magnitude of this product is small, the relationship between σ_M and the RMS DGD is a function of the exact shape of the low coherence source, see [8].

(*I(t)* is the amplitude of the delay histogram and *t* is the time component). The relationship between the two is [8]

$$\langle \Delta \tau^2 \rangle^{1/2} \approx \sqrt{\frac{3}{4}}\, \sigma_M. \qquad (4)$$

The evaluation of Equation (3) should be performed with caution. There will be non-ideal features of the delay histogram that make it deviate from a true Gaussian. The most significant features are the autocorrelation peak and the noise floor (dominant at high values of *t*). The integration limits for Equation (3) must be chosen carefully in order to exclude these unwanted features, but this must be done iteratively so as not to incur a bias in the opposite direction due to excluding real data. Examples of procedures to correctly extract $\langle \Delta \tau^2 \rangle^{1/2}$ from a mode-coupled interferogram are provided in [9] and [10].

PMD measurements using low-coherence interferometry have several advantages over other techniques. The measurements can be done quickly–the time required is essentially the travel time of the interferometer mirror over the desired scan range (a few seconds). Unlike most of the frequency-domain techniques, low-coherence interferometry does not require numerical comparison between data sampled at two different points in time. This makes interferometry less susceptible to dynamic changes in the measurement path (such as movement of the fiber leads). The biggest disadvantage of low-coherence interferometry is the need to use a spectrally broad source, which precludes measurements in a narrow passband.

Another aspect of PMD measurements made using low-coherence interferometry is the effect of multipath interference (MPI). Multiple reflections within the measurement path will cause delays in the signal transmission and show up on the delay histogram indistinguishable from delays due to PMD. While it may be useful to measure these MPI effects, the user should be aware that low-coherence interferometry is unable to distinguish between MPI and PMD.

IV. Frequency-Domain Measurements.
PMD measurements based in the frequency domain measure the same DGD as time-domain measurements but from a different perspective. The most common approach to DGD measurement in the frequency domain involves a differential method where the difference in propagation delay between light traveling on the fast and slow PSP is measured by assessing its effect on the polarization state of light as it exits the test device. The polarization dispersion vector **Ω** is related to the change in output polarization state **S** as [11]

$$\frac{d\mathbf{S}}{d\omega} = \mathbf{\Omega} \times \mathbf{S}, \qquad (5)$$

where ω is the optical frequency of the light. The physical meaning of this expression is that PMD in a device causes the output polarization state to precess about the polarization dispersion vector (PSP) as the optical frequency is changed (Figure 7).
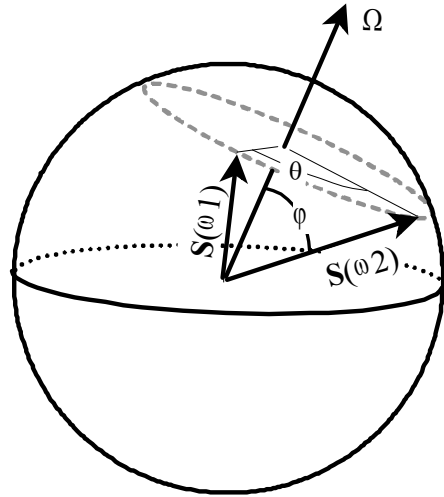

Figure 7. Poincaré sphere representation of polarization dispersion vector **Ω** and output polarization state **S** at optical frequencies ω₁ and

From Equation (5), the precession rate will be equal to the DGD of the device:

$$\left| \frac{d\theta}{d\omega} \right| = |\mathbf{\Omega}| = \Delta \tau, \qquad (6)$$

where θ is defined in Figure 7 as the angle of rotation of the output state of polarization about the precession axis **Ω**. The DGD can be found by measuring Δθ/Δω (as an approximation to *dθ/dω*). The class of frequency-domain techniques which measure

$\Delta\theta/\Delta\omega$ will be referred to as "polarimetric techniques".

The distinction between the various polarimetric techniques is how they measure $\Delta\theta/\Delta\omega$. The techniques all begin with launching polarized light into the test device and measuring the output state as a function of optical frequency $S(\omega)$. The change in S with frequency yields $\Delta S/\Delta\omega$ (not $\Delta\theta/\Delta\omega$), and this is where the variation in approaches comes in.

Three very similar techniques of polarimetric measurement of DGD will be discussed here – Jones Matrix Eigenanalysis (JME) [12], Müller Matrix Method (MMM) [13], and Poincaré Sphere Analysis (PSA) [14, 15]. All three offer robust means of assessing $\Delta\tau$ from the wavelength dependence of the output polarization state, and all three can be measured using the same experimental setup (Figure 8). These three techniques find both DGD and the PSP by measuring the wavelength-dependent rotation of the output polarization state.
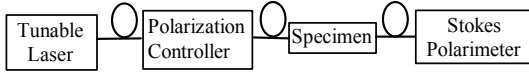

Figure 8. General diagram of experimental setup for JME, MMM, and PSA measurement techniques.

JME Technique: The JME technique gives a robust measurement of $\Delta\theta/\Delta\omega$ and Ω by turning the measurement into an eigenvalue problem [12]. At a given optical frequency ω_1, three noncollinear input polarization states (such as linearly polarized with 0°, 45°, and 90° orientations) are input to the device and the corresponding output polarization states are measured. This allows the 2×2 Jones transfer matrix $T(\omega_1)$ to be calculated following Reference [16]. ($T(\omega_1)$ is the matrix that describes the transformation of the input polarization state to the output polarization state at the optical frequency ω_1, $S_{out}(\omega_1)=T(\omega_1)S_{in}$.) Then the same three states are launched at a slightly different optical frequency ω_2 and $T(\omega_2)$ is calculated. The product $\Gamma(\varpi, \Delta\omega)=T(\omega_1)T^{-1}(\omega_2)$,

where Γ, which depends on the average optical frequency $\varpi=(\omega_1+\omega_2)/2$, and on the frequency step size $\Delta\omega=\omega_2-\omega_1$, describes the evolution (precession) of the output polarization state about the PSP. That is, $S_{out}(\omega_2)=\Gamma(\varpi,\Delta\omega)S_{out}(\omega_1)$. The eigenvectors of Γ are the PSP, and the two eigenvalues are $\rho_q=\exp(i\tau_{g,q}\Delta\omega)$, where the index q denotes propagation along the fast or slow axis and $\tau_{g,q}$ is the associated group delay. The DGD is then

$$\Delta\tau(\varpi) = \left|\tau_{g,f} - \tau_{g,s}\right| = \left|\frac{Arg(\rho_f / \rho_s)}{\Delta\omega}\right|. \quad (7)$$

Thus, JME allows the full $\Omega(\varpi)$ to be calculated, even for highly mode-coupled devices.

MMM technique: The Müller Matrix Method (MMM) [13] measures PMD in much the same way as the JME technique, but with a few simplifications. The MMM works entirely in Stokes space, with measurements of the output polarization state S and the calculation of the 3×3 polarization transfer matrix R all performed in Stokes space. JME typically measures S in Stokes space and calculates the 2×2 transfer matrix in Jones space. Second, the MMM technique measures the polarization transfer matrix by using only two launched states (JME uses three). These two states can simply be two different linear polarizations (the angle between them is not important to the measured value, but will have an effect on the measurement noise). Finally, this two-state characterization of the transfer matrix assumes no polarization-dependent loss (PDL) is present; JME does not make this explicit assumption.

Similarly to JME, the MMM technique measures the polarization transfer matrix R at two closely spaced optical frequencies, yielding $R(\omega_1)$ and $R(\omega_2)$, and calculates $R_\Delta = R(\omega_2)R^T(\omega_1)$. Since there is assumed to be no PDL, R and R_Δ are treated as pure rotation matrices, meaning $R^T=R^{-1}$, so, under this assumption, R_Δ is equivalent to Γ from the JME case. The difference is that R_Δ is a 3×3 matrix in Stokes space and Γ is a 2×2 Jones matrix. If R_Δ is a pure rotation

matrix, the precession angle θ of the output polarization state will be given by

$$\cos(\theta) = \frac{1}{2}(\mathrm{Tr}\mathbf{R}_\Delta - 1), \qquad (8)$$

where $\mathrm{Tr}\mathbf{R}_\Delta$ is the trace of $\mathbf{R}_\Delta$; the PSP (rotation axis) can be found as the eigenvector of $\mathbf{R}_\Delta$ that corresponds to an eigenvalue of 1 [17]. This is detailed in [13].

PSA Technique: The differences between the JME and PSA techniques occur only in the data analysis. Not only can the same experimental setup be used, but the same measurement procedure can be followed. The PSA technique works with derivatives of the measured Stokes vectors rather than the polarization transfer matrix. For linear-polarization launch states at approximately 0°, 45°, and 90°, the corresponding output polarization states are measured at two closely spaced wavelengths. Vector products of these three states are used to form four output Stokes vectors $\mathbf{h}$, $\mathbf{q}$, $\mathbf{c}$, and $\mathbf{c}'$, such that the finite change due to wave-length of each, $\Delta\mathbf{h}$, $\Delta\mathbf{q}$, $\Delta\mathbf{c}$, and $\Delta\mathbf{c}'$, gives the DGD [14, 15]

$$\Delta\tau = \frac{1}{\Delta\omega}\arcsin\left(\frac{1}{2}\sqrt{\frac{1}{2}\left(\Delta\mathbf{h}^2 + \Delta\mathbf{q}^2 + \Delta\mathbf{c}^2\right)}\right) +$$
$$+ \frac{1}{\Delta\omega}\arcsin\left(\frac{1}{2}\sqrt{\frac{1}{2}\left(\Delta\mathbf{h}^2 + \Delta\mathbf{q}^2 + \Delta\mathbf{c}'^2\right)}\right).$$

$$(9)$$

PSA also allows calculation of the PSP using the same four vectors.

PA, SOP, and PS: Various other polarimetric measurement techniques with similarities to JME, PSA, and MMM are sometimes mentioned. But their names generally come up under the topic of "Other measurement techniques". These techniques, Poincaré Arc (PA), State of Polarization (SOP) and Poincaré Sphere (PS) are often mentioned without literature references and so, it is difficult to define a measurement procedure to associate with each name. A good generalization would be to use these somewhat generic titles to refer to techniques that measure the DGD by measuring $\Delta\mathbf{S}/\Delta\omega$ only. This requires the assumption that,

$$\left|\frac{dS}{d\omega}\right| = \left|\frac{d\theta}{d\omega}\right|. \qquad (10)$$

This is true when $\mathbf{S}(\omega)$ lies on a great circle, and occurs when an input polarization state is launched so that both PSP are equally illuminated. This condition is difficult to maintain in a mode coupled device such as a long fiber, but is possible in non-mode-coupled components. As an example, a $\Delta\tau = 1$ ps device would have an arc of $\sim 45°$ for a wavelength change of 1 nm.

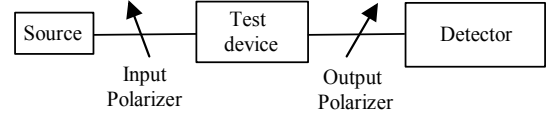**Figure 9.** Diagram of fixed analyzer setup.

Fixed Analyzer: A simple, but different approach for a polarimetric measurement technique in the frequency domain is the Fixed Analyzer (FA) method [18]. It is sometimes called Wavelength Scanning. The FA technique measures mean DGD based on Equation (6), but indirectly. Figure 9 illustrates the basic setup. Light transmitted through a polarizer - test device - polarizer setup is detected as a function of wavelength. This can be done either with a tunable laser and detector combination or with a broadband source and an optical spectrum analyzer (or monochromator). As the output polarization vector $\mathbf{S}$ moves around on the sphere, the intensity $I(\omega)$ transmitted through the output polarizer of Figure 9 is proportional to the quantity $1+\sin(\theta)\sin(\varphi)\cos(\Phi)$, where Φ is the angle between $\mathbf{\Omega}$ and Stokes vector describing the axis of the output polarizer, and φ is the angle between $\mathbf{S}$ and $\mathbf{\Omega}$ (Figure 7), and is independent of ω for non-mode-coupled devices. For non-mode-coupled devices, $\theta(\omega)$ depends approximately linearly on ω and contains all of the optical frequency dependence of $I(\omega)$, and so we can estimate $d\theta/d\omega$ (and thus average DGD $\langle\Delta\tau\rangle$) by merely counting the number of extrema (peaks and valleys) in the sinusoidal $I(\omega)$ curve over a given optical frequency range. That is,

$$\langle\Delta\tau\rangle_{\omega_a - \omega_b} = \frac{k\,N_e\pi}{\omega_b - \omega_a} = \frac{k\,N_e\lambda_a\lambda_b}{2(\lambda_a - \lambda_b)c}, \quad (11)$$

where the brackets indicate the average DGD measured over the frequency range from ω_a to ω_b, k is a mode-coupling constant (equal to 1 for non-mode-coupled devices), N_e is the number of peaks and valleys measured over the frequency range from ω_a to ω_b. The right-most expression in Equation (11) is merely the same expression in terms of wavelength instead of optical frequency.
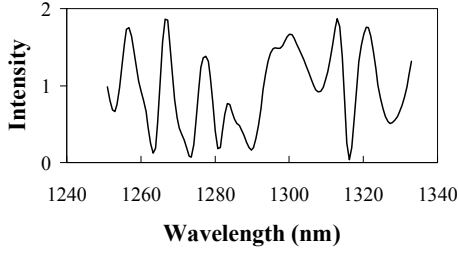

Figure 10. Typical spectrum from fixed analyzer measurement of non-mode-coupled device.

If we consider the case of a mode-coupled device, the situation becomes more complicated in that $d\theta/d\omega$ can depend strongly on ω, and Ω can also have a second-order dependence ω (Ω is still independent of ω to first order). This means that $I(\omega)$ no longer has a simple sinusoidal dependence but behaves in a quasi-random way as shown in Figure 10. Fortunately, the mean DGD can still be estimated by counting peaks and valleys in the $I(\omega)$ spectrum. In this case, the coupling factor k becomes 0.805. k comes from a Monte Carlo simulation and allows an accurate estimate of mean DGD when the device is strongly mode-coupled [19].

Evaluating the mean DGD from $I(\omega)$ is straightforward for a non-mode-coupled device since it merely involves counting peaks and valleys of a sinusoidal signal. However, in the case of mode-coupled devices, it can become difficult to distinguish peaks and valleys from intensity noise. Often a "thresholding" algorithm is used to ignore peaks and valleys whose extent is less than some defined fraction of the full-scale excursion of $I(\omega)$. This practice will incur a bias due to ignoring some fraction of real peaks and can easily give ~10 %

errors. This problem is discussed and a lookup-table correction factor is suggested to reduce this bias in [19]. FA measurements on mode-coupled devices can also be biased by sampling too coarsely (causing small peaks to be missed, thus underestimating the mean DGD). In order to sufficiently sample I(ω), a device of nominal mean DGD $\langle\Delta\tau\rangle$ should be measured with at least $2\langle\Delta\tau\rangle\Delta\omega$ frequency points for a measurement spectrum of $\Delta\omega$ [19].

An alternative evaluation of the FA spectral data is often used. Rather than calculating $\langle\Delta\tau\rangle$ from a $d\theta/d\omega$ estimate based on counting peaks and valleys, the $I(\omega)$ spectrum can be Fourier-transformed into the time domain. The result is a "delay histogram" very similar to that which would be seen for a low-coherence interferometric measurement with the same source spectrum as used in the FA measurement (windowing is often used to optimize the results). The mean DGD can then be evaluated in the time domain by the same means as with low-coherence interferometry [20].
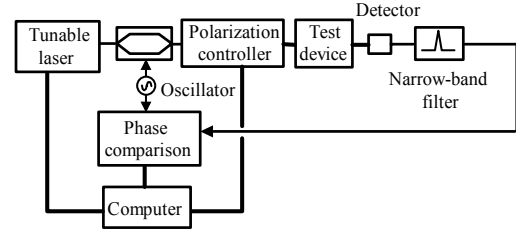

Figure 11. Generic diagram of experimental setup for RF phase shift measurement system.

RF Phase Shift: The final technique to be discussed resembles the time-of-flight measurement. Figure 11 illustrates a typical setup. A tunable laser is intensity modulated at a frequency ranging from several tens of MHz to a few GHz. The modulated light passes through a polarization controller and then the test device and is then detected. The phase of the detected signal is compared to the phase of the modulator as the polarization state of the light is changed. The arrival phase φ_{RF} is related to the time of flight through the device, so that as the input polarization state is changed, the maximum and minimum phase meas-

ured $\varphi_{RF,max}$ and $\varphi_{RF,min}$ can be used to find the maximum and minimum polarization-dependent propagation delays through the device. Their difference gives the Differential Group Delay through the test device,

$$\Delta\tau = \frac{\varphi_{RF,max} - \varphi_{RF,min}}{360° \cdot f_{mod}}, \qquad (12)$$

where phases are given in degrees and f_{mod} is the RF modulation frequency [21]. The down side of this intuitive approach is that it requires many phase measurements while the polarization state is randomly varied to find the maximum and minimum. This approach is improved by algorithms that allow $\Delta\tau$ to be obtained by measuring the RF phase at just four known polarization states (launched at points orthogonal to each other on the Poincaré sphere). Two such implementations are the Modulation Phase Shift (MPS) technique [22] and Polarization-dependent Signal Delay (PSD) method [23]. The PSD technique offers the advantage of calculating both the DGD and the PSP. RF phase shift is a promising technique in that it allows narrowband measurements whose spectral width is due to only the RF modulation frequency.

The classification of the RF phase shift techniques as frequency-domain is somewhat ambiguous. The distinction between the time and frequency domains relies on the coherence length of the optical source, but in principle, the MPS and PSD techniques will work with either a spectrally narrow laser source or a broadband source. The choice to include RF techniques in the frequency domain is therefore based on the coherence time of the RF modulation.

V. Experimental Setup Details

Inherent Lead PMD: When making a PMD measurement, it is important that there be no stray PMD in the measurement system or the fiber leads. The leads connecting the measurement system to the device being tested can have inherent birefringence (due to asymmetries or stresses from the manufacturing process), which leads to PMD. The DGD due to these stresses will be a few femtoseconds for lead lengths of a few meters. Selecting low-PMD leads and using the shortest lengths possible will minimize errors due to lead birefringence.

Bend-induced PMD in Leads: Even low-PMD leads can exhibit significant PMD under bending, which causes a stress-induced birefringence. This bend-birefringence increases like r^{-2}, where r is the radius of the fiber bend [24]. Extending this to DGD, we find the bend-induced DGD goes like 1/r. Measurements should be made with the fiber leads as short and straight as possible.

Once lead PMD has been minimized, it is best to measure the remaining PMD of the measurement system by removing the test device, connecting the leads together and measuring the "system DGD." Since PMD is a vector quantity, the device PMD and the system PMD will not simply add as scalars, but as vectors. The combined PMD will depend on the relative orientations between the PSP axis within the leads and the PSP axis of the test device. In other words, the final measurement cannot be corrected by simply subtracting the measured value for system DGD. The best solution is to measure the device several times with the leads re-oriented in between each measurement (avoiding small bend radii). The average of these multiple measurements will give the best estimate of the device DGD. This final value will still have effects due to system birefringence; but, they can be documented by including the system DGD in the uncertainty statement for the device.

Stabilizing the Measurement: Care should be taken before the measurement to stabilize both the measurement system and the test device against temperature changes or movement. Even fiber leads having only a small amount of DGD can have a big effect on measurement noise if they are moving during the measurement. This is particularly important for the polarimetric measurement techniques, which measure the output polarization state of the light in order to determine the DGD. A moving fiber lead can change the output polarization state significantly, which results in a DGD error

proportional to the total DGD being measured (not just the DGD of the leads). Similarly, for MPS and PSD techniques, where the measured DGD comes from 4 measurements separated in time from each other, moving fiber leads can cause errors proportional to the total DGD. In the case of low-coherence interferometry, the polarization state is not directly measured, and the light propagating down different polarization states of the test device is detected simultaneously, so there is much less effect from moving fiber leads. In general, for all measurements, it is best it is best to secure the fiber leads against motion during measurements.

Temperature should also be kept stable during a measurement − even for devices with relatively a low temperature dependence of their DGD. The reason for this is the same as with the moving fiber leads. A change in temperature of the device will change the birefringence slightly, causing the polarization state to change with time, which produces a DGD noise proportional to the total DGD of the measurement. This can be seen in Figure 12, where a simple quartz plate element was measured as the temperature went from room temperature to ~40 °C in about 30 minutes. From the graph, it is clear that when the temperature is held constant, there is little difference between the measured DGD at room temperature and the elevated temperature (we measured a temperature coefficient of approximately 0.08 fs/°C). However, during the transition between room temperature and the elevated temperature, the DGD varied significantly. This illustrates the importance of a stable temperature environment for the measurement. It is best if devices can be held at a constant temperature or at least insulated to cause any temperature changes to occur slowly. Again, it is expected that this effect on the DGD will be greater for frequency domain measurements and less for interferometric measurements.

Multipath Interference: When multiple reflections occur within the measurement path, a cavity is set up where a fraction of the light passing through the cavity receives extra delay. This will show up on an interferometric measurement and be indistinguishable from DGD. This will also show up as a ripple on FA spectra (in the absence of source normalization) that could be mistaken for higher DGD values. In the rest of the frequency-domain measurements, the measured DGD will be affected by multiple reflections only if the cavity contains DGD. In that case, the DGD spectrum will have a ripple whose amplitude is dependent on the amount of DGD within the cavity and the strength of the reflections. The period of these multiple-reflection-induced ripples will come from the cavity spacing. When there is DGD in the cavity, there will be two spacings − one associated with the fast PSP and the other with the slow PSP. These two closely spaced periodicities will result in a beat note in the ripple with a period corresponding to the DGD in the cavity.
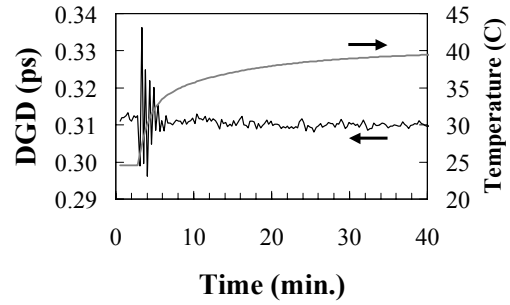

Figure 12. Measured DGD versus time for a quartz plate as the temperature is changed.

VI. Spectral Efficiency

An important figure of merit for a given PMD measurement technique comes from the DGD-bandwidth product. For all measurements, there is a trade-off between the spectral bandwidth in which the measurement is made and the DGD resolution achievable. We define a "Bandwidth Efficiency Factor" α that relates the DGD-bandwidth product to the achievable signal to noise ratio (SNR) as

$$SNR \leq \alpha \, \Delta\tau \, \Delta\omega, \qquad (13)$$

where $\Delta\tau$ is the DGD of the device and $\Delta\omega$ is the frequency spectrum used by the measurement. This relationship illustrates that for a given measurement, the SNR can

be improved by increasing the measurement bandwidth. Or, given a measurement system with a fixed measurement bandwidth requirement, the SNR is better when measuring large DGDs. α is dependent on the particular measurement technique and often on the quality of the equipment. It is useful for comparison purposes to identify "typical" values of α for the different techniques.

For the FA technique (extremum counting), α is limited by the fact that for a determination of $\langle\Delta\tau\rangle$ to be made, at least two extrema must be present in the measurement spectrum. From Equation (11), this means that the minimum DGD-bandwidth product will be $\langle\Delta\tau\rangle\Delta\omega = \pi$, giving an SNR of 1, so $\alpha=1/\pi$. This value could be improved by the use of a different evaluation technique (such as analyzing multiple level crossings as opposed to only peaks and valleys [25]). In the case of the FA technique evaluated with the Fourier transform, or equivalently a low-coherence interferometric measurement, the DGD resolution is limited by the coherence time T_c of the broadband source. For a Gaussian source spectrum, $T_c \approx 4/\Delta\omega$ [7]. If the DGD resolution is limited by T_c, then we have a SNR of 1 when $\Delta\tau\Delta\omega=T_c\Delta\omega=4$, giving $\alpha = 1/4$ for low coherence interferometry (or a Fourier transform evaluation of an FA technique with a Gaussian source). Polarimetric techniques will generally have their bandwidth efficiency limited by noise in the polarization-sensitive detection. Since $\Delta\theta/\Delta\omega$ is used as the measure of DGD, the noise on the $\Delta\theta$ measurement and the noise on the $\Delta\omega$ measurement both affect α. If a wavelength meter is used in the measurement, uncertainty on $\Delta\omega$ will be small, and the effective noise associated with the angular change in the output polarization state $\delta\Delta\theta$ will dominate (for small values of $\Delta\tau$). So, SNR can be estimated to be $\Delta\theta/\delta\Delta\theta=\Delta\tau\Delta\omega/\delta\Delta\theta$. Comparing with Equation (13) yields $\alpha = 1/\delta\Delta\theta$. For comparison purposes, achievable values of α for a JME technique can be ~250. Finally, for the RF-based techniques of MPS and PSD, the measurement bandwidth is determined by the modulation frequency, and the measurement noise is fundamentally limited by the phase resolution $\Delta\varphi$ of the phase-sensitive detector (lock-in amplifier, vector voltmeter, or network analyzer). Defining the DGD resolution as the time delay corresponding to the phase resolution, we find the bandwidth efficiency factor for RF phase-shift-based techniques to be

$$\alpha = \frac{360°}{4\pi\,\Delta\varphi_{\text{deg}}}, \qquad (14)$$

where $\Delta\varphi_{\text{deg}}$ is in degrees. For an achievable 0.02° phase resolution, this gives a value of $\alpha=1432$.

The bandwidth efficiency factor is useful in the measurement of narrowband components where measurement precision is needed in a small spectral bandwidth. α can be used to estimate the achievable resolution given the available bandwidth. For example, if a measurement technique with an α of 250 is used to measure the nominally 0.1 ps DGD of a filter with a usable bandwidth of 50 GHz, the best achievable signal-to-noise ratio (SNR) can be found as follows. The 50 GHz bandwidth allows a maximum frequency step size of $\Delta\omega=2\pi\cdot50$ GHz $= 3\times10^{11}$ rad/s, and using Equation (13) with $\Delta\tau = 0.1$ predicts a maximum SNR of 7.5 or 13 % noise.

VII. Wavelength Step Size
If spectral resolution and available bandwidth are not limiting factors, it is attractive to use a larger frequency step size in the measurement to improve the DGD resolution. Since most frequency-domain measurement systems can easily vary the spectral resolution, it is important to be aware of the tradeoffs. For polarimetric techniques, which determine DGD through measurement of $\Delta\theta/\Delta\omega$, it is important to note that $\Delta\theta$ is known only to within a factor of 2π, and the determination of $\Delta\theta/\Delta\omega$ can suffer from ambiguities such as aliasing if $\Delta\theta$ is greater than π for the given frequency step $\Delta\omega$. This has implications in all the frequency-domain measurement techniques and can be expressed as the requirement

$$\Delta\tau\Delta\omega \le \pi, \qquad (15)$$

or, in terms of wavelength, measurements cannot be trusted unless

$$\Delta\tau\Delta\lambda \le 4\,\text{ps}\cdot\text{nm}, \qquad (16)$$

where, for Equation (16), $\Delta\tau$ is in units of picoseconds and $\Delta\lambda$ in nanometers and a nominal 1550 nm operating wavelength is assumed. In order to take into account variations in DGD with wavelength, $\Delta\tau$ in Equations (14) and (15) should represent the maximum DGD over the measurement range (not just the average). The need to resolve changes in DGD requires a further increase in the spectral sampling density. As Figure 13 shows, sufficient points must be measured to resolve the variations in DGD with wavelength. Multiple simulations on mode-coupled devices of various mean DGD values show that due to the presence of second-order effects (wavelength-dependent DGD and PSP), the sampling density must be higher than for non-mode-coupled artifacts. Figure 13 shows that increased sample density gives a more accurate estimate of the mean DGD in a mode-coupled device. For example, to measure a mean DGD that is ~95 % of the true value, the sampling density must be such that

$$\Delta\tau\Delta\lambda \le 1.5 \text{ ps}\cdot\text{nm}, \qquad (17)$$

(at 1550 nm), where again $\Delta\tau$ is in picoseconds and $\Delta\lambda$ is in nanometers. This is a stricter requirement than the common expression in Equation (16).
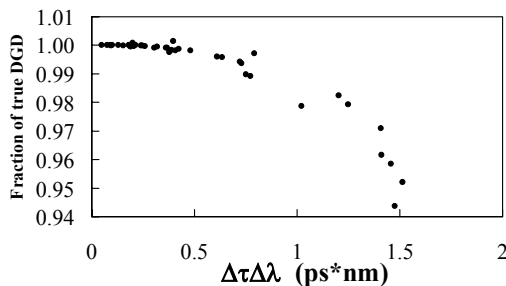

Figure 13. Simulated results of measured DGD as a function of sample density (vertical axis shows the fraction of the true DGD that is reported).

VIII. Conclusions

In measuring PMD, the first choice to be made is deciding which measurement tech-nique to use. Here, the various techniques have been described so as to illustrate their relative merits. Generally, decisions are made based on measurement time, spectral resolution, and what quantities are measurable. Once a measurement technique is chosen, it is most important to understand the sources of measurement error (and minimize them). The most significant of these have been described here.

References

[1] Paul A. Williams, "Mode-coupled artifact standard for polarization-mode dispersion: Design, assembly, and implementation," *Appl. Opt.* **38**, 6498-6507 (1999).
[2] N. Gisin, B. Gisin, J.P. Von der Weid, R. Passy, "How accurately can one measure a statistical quantity like polarization-mode dispersion?" *IEEE Photonics Tech. Lett.*, **8**, 1671-1673 (1996).
[3] Dennis Derickson, *Fiber Optic Test and Measurement*, (Prentice Hall, New Jersey, 1998).
[4] C.D. Poole, and C.R. Giles, "Polarization-dependent pulse compression and broadening due to polarization dispersion in dispersion-shifted fiber", *Opt. Lett.*, **13**, 155-157 (1987).
[5] Yoshinori Namihira and Jun Maeda, "Polarization mode dispersion measurements in optical fibers", *Tech. Dig. – Symp. on Opt. Fiber Meas.*, Boulder, 145-150 (1992).
[6] Bamdad Bakhshi, et al., "Measurement of the Differential Group Delay in Installed Optical Fibers Using Polarization Multiplexed Solitons," *IEEE Phot. Tech. Lett.*, **11**, 593-595 (1999).
[7] Joseph W. Goodman, *Statistical Optics*, (Wiley, New York, 1985) p168.
[8] B.L Heffner, "Influence of optical source characteristics on the measurement of polarization-mode dispersion of highly mode-coupled fibers", *Opt. Lett.*, **21**, 113-115, (1996).
[9] P.A. Williams, "Accuracy issues in comparisons of time- and frequency-

domain polarization mode dispersion measurements", Tech. Dig. – *Symp. on Opt. Fiber Meas.*, Boulder, 125-129 (1996).

[10] TIA/EIA FOTP-124. 1999. *Polarization-mode dispersion measurement for single-mode optical fibers by interferometric method.* Telecommunications Industry Association, Arlington, VA.

[11] C.D. Poole, et. al., "Polarization dispersion and principal states in a 147 km undersea lightwave cable," *J. of Lightwave Tech.*, **LT-7**, 1185-1190 (1989).

[12] B.L. Heffner, "Automated Measurement of Polarization Mode Dispersion Using Jones Matrix Eigenanalysis," *IEEE Photonics Tech. Lett.*, **4**, 1066-1069 (1992).

[13] R.M. Jopson, "Measurement of Second-Order Polarization-Mode Dispersion Vectors in Optical Fibers," *IEEE Photonics Tech. Lett.* **11**, 1153-1155 (1999).

[14] Normand Cyr, et al., "Stokes Parameter Analysis Method, the Consolidated Test Method for PMD Measurements," *Proceedings Nat. Fib. Opt. Eng. Conf.*, Chicago, (1999).

[15] TIA/EIA FOTP-122. 1999. *Polarization-Mode Dispersion Measurement for Single-ModeOptical Fibers by Stokes Parameter Evaluation.* Telecommunications Industry Association, Arlington, VA.

[16] R. Clark Jones, "A New Calculus for the Treatment of Optical Systems: VI. Experimental Determination of the Matrix," *J.O.S.A.* **37**, 110-112 (1946).

[17] Mary L. Boas, *Mathematical Methods in the Physical Sciences* (Wiley, New York, 1983) p.454.

[18] Craig D. Poole, "Polarization-Mode Dispersion Measurements Based on Transmission Spectra Through a Polarizer," *J. Lightwave Tech.*, **12**, 917-929 (1994).

[19] P.A. Williams and C.M. Wang, "Corrections to Fixed Analyzer Measurements of Polarization Mode Dispersion," *Journal of Lightwave Technology*, **16**, 534-541 (1998).

[20] B.L. Heffner, "Single-mode propagation of mutual temporal coherence: equivalence of time and frequency measurement of polarization-mode dispersion," *Opt. Lett.*, **19**, 1104-1106 (1994).

[21] P.A. Williams et. al., "Narrowband measurements of polarization-mode dispersion using the modulation phase shift technique," *Tech. Dig. – Symp. on Opt. Fib. Meas.*, Boulder, 23-26 (1998).

[22] P.A. Williams, "Modulation phase-shift measurement of PMD using only four launched polarization states: a new algorithm," *Elec. Lett.*, **35**, 1578-1579 (1999).

[23] Lynn E. Nelson, et. al. "Measurement of polarization mode dispersion vectors using the polarization-dependent signal delay method," *Opt. Express*, **6**, 158-167 (2000).

[24] Luc B. Jeunhomme, Single-Mode Fiber Optics: Principles and Applications, (Marcel Dekker Inc, New York, 1983) p. 66.

[25] A. Galtarossa et al., "Accuracy Enhanced PMD Measurements with Wavelength Scanning Technique", *Tech. Dig. – Optical. Fib. Meas. Conf.*, Nantes 45-48, (1999).